# EIS vs. Dynexus Technology's iRIS®

## Introduction

Standard Electrochemical Impedance Spectroscopy (EIS) has been recognized as a valuable diagnostic sensor for battery diagnostics and prognostics. It consists of sequentially exciting a battery over a frequency range and capturing the response. The resulting data can be used to identify changes in the bulk behavior of electrochemical processes due to changes in temperature, voltage, health, or stability.[1,2] Figure 1a shows example impedance spectra plotted in a Nyquist curve for a fresh lithium-ion cell. The point at which the spectrum crosses the real axis on the left side is the ohmic resistance, which is influenced by the electrolyte, separator, tabs, contact resistance, etc. The mid frequency region (e.g., between ~300 Hz and ~1 Hz) is the charge transfer resistance, which is influenced by kinetic reactions at the electrodes (i.e., anode and cathode). Lower frequencies on the right side of the spectra (e.g., below ~1 Hz) is the Warburg impedance that is influenced by the diffusion of ions.[2] Battery state of charge, state of health, and state of stability correlates with these impedance metrices.[2,3]

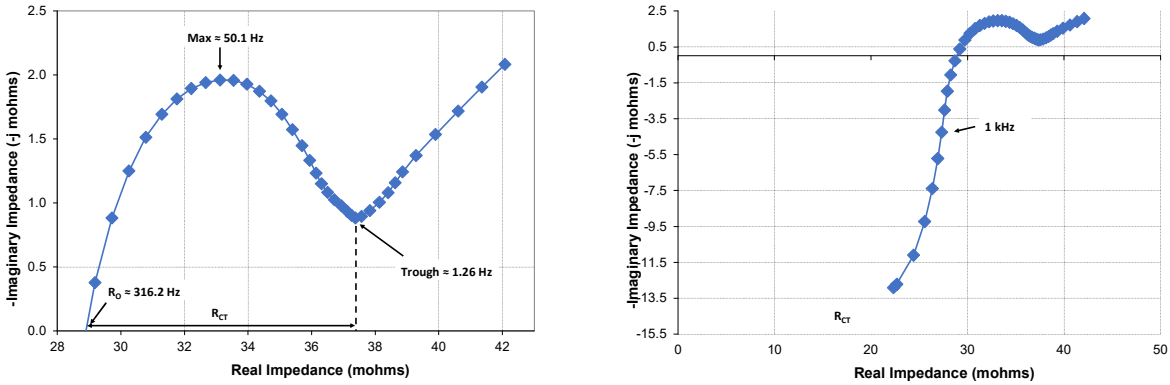


(a) (b)

**Figure 1.** (a) Standard AC impedance measurements and (b) full spectrum plot

Standard EIS has been difficult to implement as a field-deployable sensor since commercial systems are expensive, bulky, and a measurement can take 10-minutes to an hour (depending on system settings), which is impractical for assessing large production volumes or generating in-use datasets for enhanced diagnostics and prognostics. Consequently, emphasis in the literature has generally been placed on using a single frequency measurements.[2,4] However, one frequency provides very limited data which does not reveal all the key electrochemical processes that happens in a battery at different time scales. Typical single-frequency measurements are conducted at 1 kHz for rapid assessments. However, as shown in Figure 1b, 1 kHz is often in the high frequency inductive tail, which may at best only provide an estimate of the ohmic resistance.

---

[1] T. Tanim et al., Advanced Diagnostics to Evaluate Heterogeneity in Lithium-ion Battery Modules, *eTransportation* 3 (2020), p.100045

[2] J. Lamb et. al., SAND2017-6959, July 2017

[3] J. Christophersen, Battery State-of-Health Assessment Using a Near Real-Time Impedance Measurement Technique Under No-Load and Load Conditions, Dissertation, Montana State University. April 2011

[4] C. Love et. al., State-of-health monitoring of 18650 4S packs with a single-point impedance diagnostic, J Power Sources, 266 (2014), 512-519

Dynexus Technology is commercializing a breakthrough in rapid, broadband impedance measurements known as inline Rapid Impedance Spectroscopy (iRIS®) for advanced battery diagnostics and prognostics. The iRIS technology was originally developed by the Idaho National Laboratory (INL) and Montana Technological University (Montana Tech). In December 2016, Dynexus entered into an exclusive licensing agreement with INL across all domains to acquire worldwide rights to the R&D 100 award-winning battery health scanning technology.

IRIS overcomes the hurdles associated with standard AC impedance with a fast, broadband impedance measurement (typically ≤10s) that is customizable for specific applications. It also can capture impedance measurements under dynamic conditions for rapid assessment at strategic battery conditions without having to interrupt a test or a load.[2,3] The iRIS system comes equipped with triggering capability as well, such that rapid measurements can be automatically initiated following key events (e.g., when a load is initiated or terminated). Thus, the iRIS sensor could be integrated into various applications where EIS would be useful, but previously considered impractical to implement (e.g., cell screening, end-of-line assessment, second-use assessments, abuse monitoring, etc.).

**EIS vs. iRIS**

The purpose of this paper is to demonstrate how the iRIS measurements compare with standard EIS results. Two chemistries were measured at the individual cell level, including lithium-iron phosphate (LFP) and Nickel-Manganese-Cobalt (NMC) cells. Additionally, two Nissan Leaf modules, connected in a 2S2P configuration were also tested. The EIS measurements were conducted with a Solartron that was connected to the batteries through a Maccor multiplexer (Versastat 4). The frequency range was 0.0125 Hz to 9929.1 Hz with 10 points per decade of frequency (i.e., 60 frequencies). The total measurement time was slightly over 20 minutes.

Table 1 provides iRIS settings for the five rapid impedance measurements that were conducted in a back-to-back sequence immediately following the EIS test. All measurements included 20% negative time, which is an extension of the excitation signal going backwards from time t = 0s (e.g., the 10-s measurement is actually 12-s long, with 2-s of negative time followed by 10-s of impedance measurements). Its purpose is to overcome any transient effects that may be present with rapid excitation prior to calculating the impedance spectrum.

**Table 1.** iRIS measurement parameters

| Measurement | Frequency (Hz) | | Measurement speed (s) | Number of Frequencies | Negative Time |
|---|---|---|---|---|---|
| | Lower | Upper | | | |
| 1 | 0.0125 | 1638.4 | 80 | 18 | 20% |
| 2 | 0.1 | 1638.4 | 10 | 15 | 20% |
| 3 | 0.2 | 1638.4 | 5 | 14 | 20% |
| 4 | 0.3 | 1228.8 | 3.33 | 13 | 20% |
| 5 | 0.8 | 1638.4 | 1.25 | 12 | 20% |

*LFP Cells*

Eight 21700 LFP cells were subjected to impedance measurements; the results for a representative cell are shown in Figure 2. Note that there are slight differences in contact resistance between the EIS and iRIS systems, thus the EIS data were shifted slightly on the real axis to line up with iRIS results (the average shift was approximately 1 mΩ). These spectra clearly demonstrate that iRIS measurements can successfully reproduce EIS results with significantly faster speeds. When the iRIS frequency range is reduced to gain more measurement speed, there is less detail on the low-frequency Warburg tail. However, the ohmic and charge transfer resistances can still be easily identified even with the 1.25-s measurement.

Figure 3a shows the measured real impedance from EIS (without the shift used to compare Nyquist curves) plotted against the corresponding iRIS results for the 80-s measurement (0.0125 to 1638.4 Hz) for all LFP cells. Since the frequencies between the two measurements did not line up exactly, the EIS frequencies closest to iRIS were used for comparisons (e.g., the EIS measurement was a 49.76 Hz, whereas iRIS was at 51.2 Hz). These data indicate a very strong linear relationship between EIS and iRIS in the real impedance. Figure 3b shows the corresponding relationship between EIS and iRIS for the imaginary impedance. In this case, there appears to be transition point around 200 Hz, where the slope of the linear fit changes. Although some of the discontinuity could be due to differences in measurement frequencies, it should also be noted that the high-frequency components are measured simultaneously with the low-frequency components during an iRIS excitation (i.e., a multi-sine excitation), whereas the EIS measurement captures high frequency data after approximately 20 minutes of low-level excitation. Thus, some of the observed differences may also be due to transient and/or electrochemical effects from prolonged excitation during EIS. Additional studies should be conducted on extended measurement times with EIS to determine its effect on cell response compared with fast iRIS excitation. Nevertheless, there is a very strong linear correlation between the EIS and iRIS imaginary impedance data. Table 2 summarizes the goodness-to-fit (i.e., $r^2$) coefficient for all eight cells. The real impedance is 0.998 or better in all cases. If all the imaginary data are included in a single fit, the $r^2$ coefficient is still >0.97, but if the higher frequencies are treated independently, the $r^2$ coefficient is 0.998 or better in all cases.

**Table 2.** Goodness-to-fit ($r^2$) coefficient for linear fits between EIS and iRIS (LFP cells)

| | **Real** | **Imaginary** | | |
|---|---|---|---|---|
| | **Full** | **Full** | **Low/Mid Frequency** | **High Frequency** |
| **LFP-A** | 0.999 | 0.980 | 1.000 | 1.000 |
| **LFP-B** | 0.999 | 0.973 | 1.000 | 1.000 |
| **LFP-C** | 0.998 | 0.986 | 1.000 | 1.000 |
| **LFP-D** | 0.999 | 0.987 | 1.000 | 0.999 |
| **LFP-E** | 0.998 | 0.983 | 0.999 | 0.999 |
| **LFP-F** | 0.999 | 0.981 | 1.000 | 0.999 |
| **LFP-G** | 0.999 | 0.978 | 1.000 | 0.998 |
| **LFP-H** | 0.998 | 0.981 | 0.999 | 0.998 |

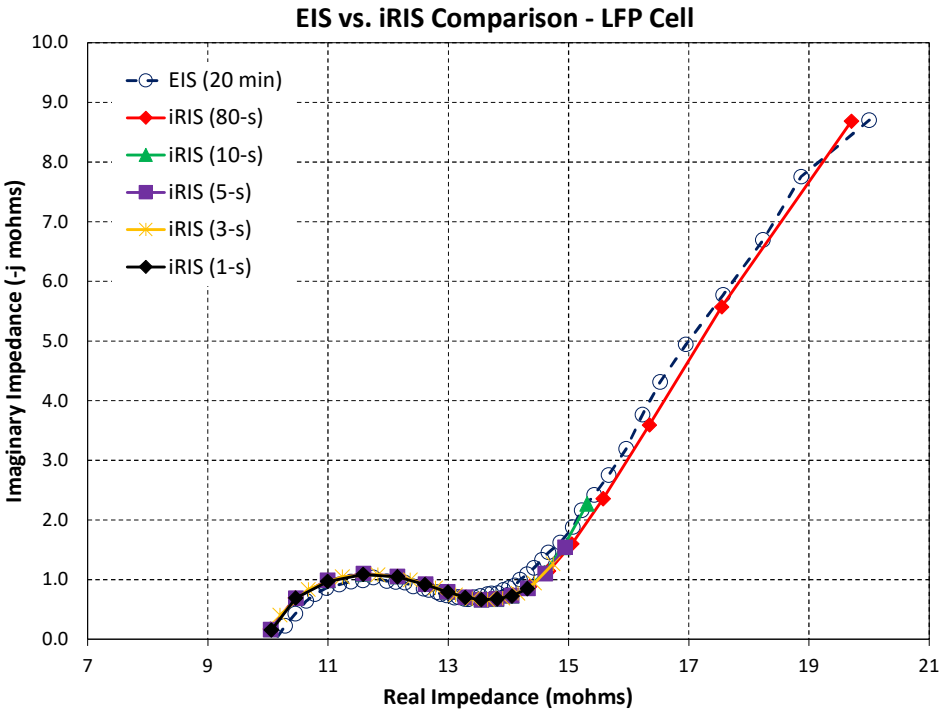


**Figure 2.** EIS vs. iRIS for a representative LFP cell

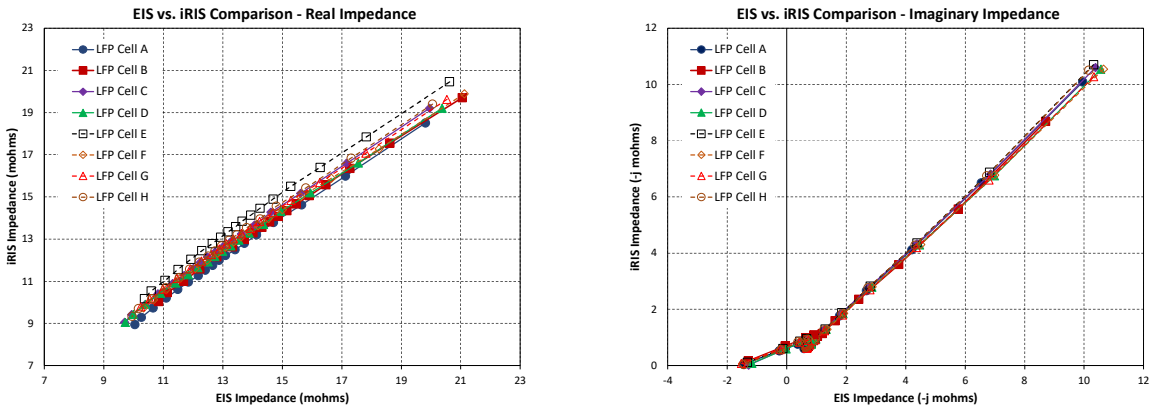


(a) (b)

**Figure 3.** Correlation between EIS and iRIS for (a) real impedance and (b) imaginary impedance

*NMC Cell*

Only one 18650 NMC cell was available for impedance measurements using the same parameters identified above. Figure 4 shows that the EIS and iRIS measurements are also very similar for this cell (the EIS data were shifted slightly due to minor variations in contact resistance). The NMC cell had been previously subjected to extensive aging and use, so the measured impedance is significantly higher compared to the LFP cells (e.g., an ohmic resistance of approximately 27 mΩ compared to an LFP ohmic resistance of about 10 mΩ). As with the LFP cells, the back-to-back iRIS measurements are highly repeatable over the common frequency range.

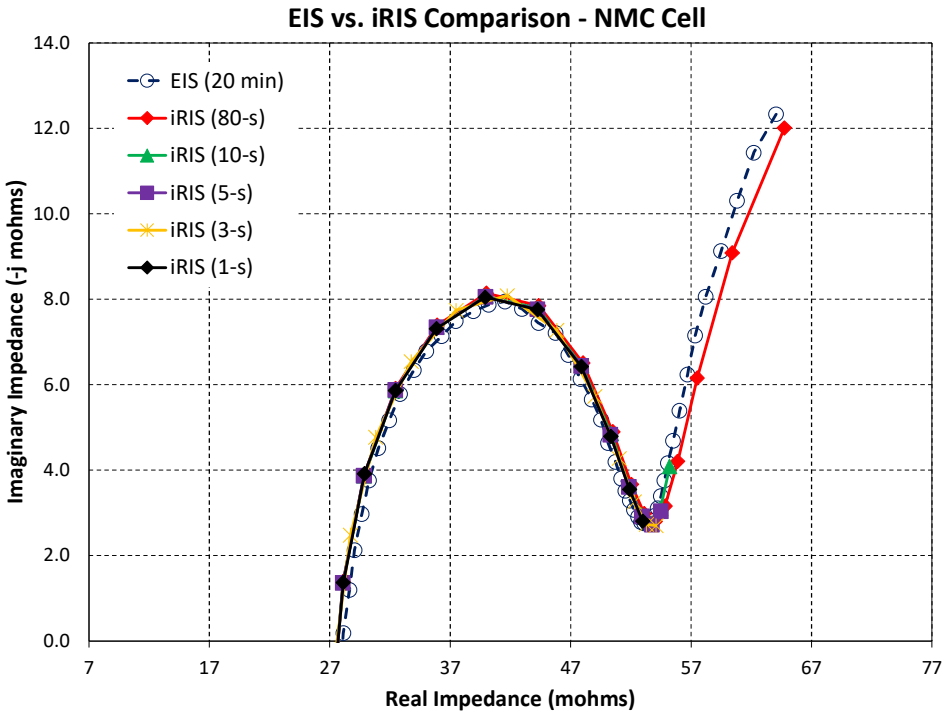


**Figure 4.** EIS vs. iRIS for a representative NMC cell

Figure 5 shows the correlation between the (a) real impedance and (b) imaginary impedance between EIS and iRIS. The $r^2$ coefficient is 1.000 for the real impedance and 0.999 for the imaginary impedance. In this case, there is no obvious separation in slope at the higher frequencies. If, however, the frequencies at 200 Hz and above are separated (as with the LFP cells), the $r^2$ coefficient is 1.000 for the low and mid frequencies and 0.999 for the higher frequencies. These data also demonstrate that iRIS can accurately reproduce an EIS curve.

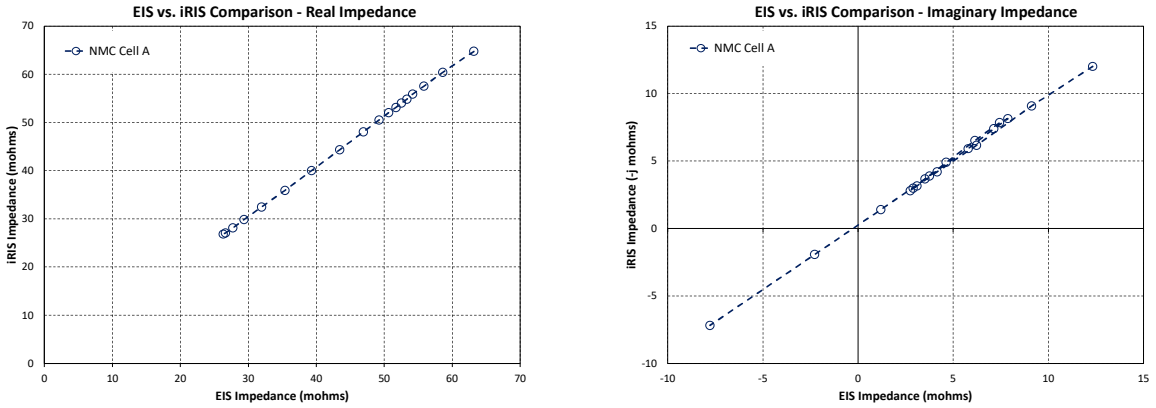


(a) (b)

**Figure 5.** Correlation between EIS and iRIS for (a) real impedance and (b) imaginary impedance

Most EIS equipment is limited to the cell-level assessments (i.e., ≤5V or less), however, newer models are coming out with higher voltage capabilities (around 10 to 12 V capabilities). The available Versastat 4 connected to the Maccor tester could measure up to 8V, so two NMC Nissan Leaf modules in a 2S2P configuration were also subjected to an EIS vs. iRIS comparison. Unlike the cylindrical LFP and NMC cells, the Leaf cells are in a pouch configuration with significantly lower impedance (the ohmic resistance for the 2S2P module is about 4.7 mΩ). Figure 6 shows the impedance spectra for a representative module (again, the EIS data were shifted slightly due to minor variations in contact resistance). Although the iRIS measurements are still very repeatable with increasing measurement speeds, the EIS system had trouble capturing the spectrum. There is significant noise in captured spectrum throughout the entire frequency range. The high-frequency inductive tail (highlighted in Figure 7) also had some discontinuities as well. It is unknown if the EIS struggled due to the higher voltage level, the lower impedance level, or both. Additional studies should be conducted to evaluate repeatability of both EIS and iRIS measurements on these Leaf modules.

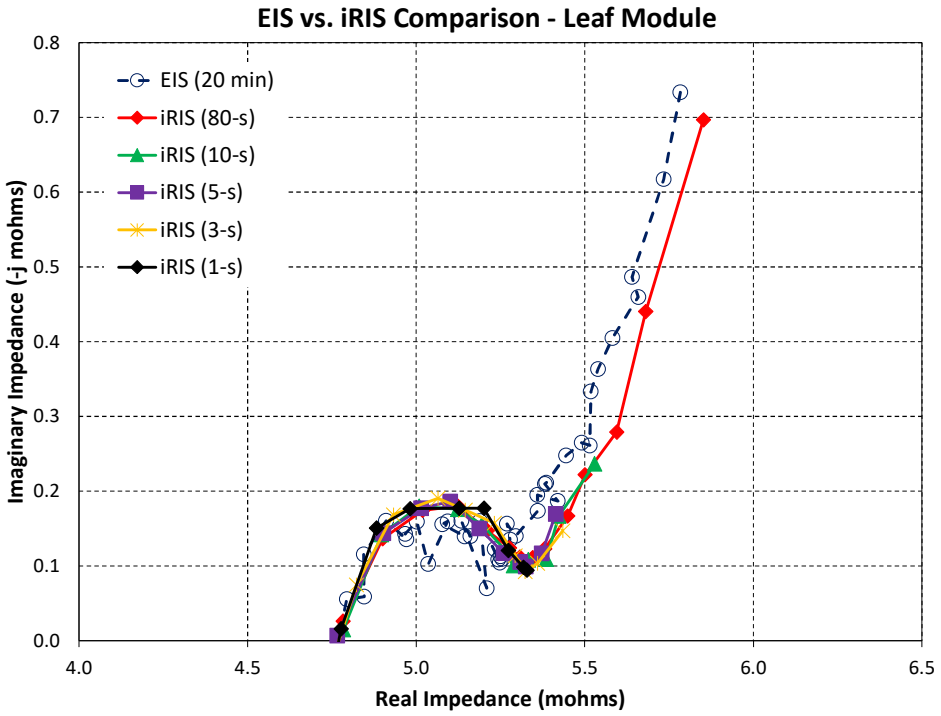


**Figure 6.** EIS vs. iRIS for a representative Leaf module

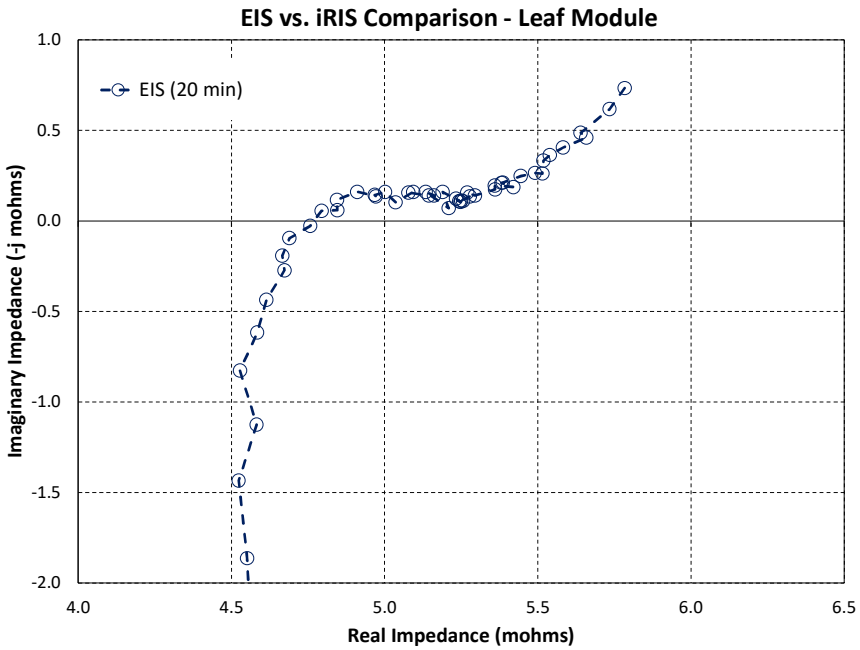


**Figure 6.** EIS high-frequency inductive tail for a representative Leaf module

Figure 8 shows the correlation between the (a) real impedance and (b) imaginary impedance between EIS and iRIS and Table 3 summarizes the $r^2$ coefficients. These data indicate that EIS struggled more with capturing the real impedance since the $r^2$ coefficients for the imaginary impedance are still near 1.

**Table 3.** Goodness-to-fit ($r^2$) coefficient for linear fits between EIS and iRIS (Leaf modules)

| | Real | Imaginary | | |
|---|---|---|---|---|
| | Full | Full | Low/Mid Frequency | High Frequency |
| **Leaf-A** | 0.984 | 0.999 | 0.986 | 1.000 |
| **Leaf-B** | 0.984 | 0.998 | 0.996 | 1.000 |

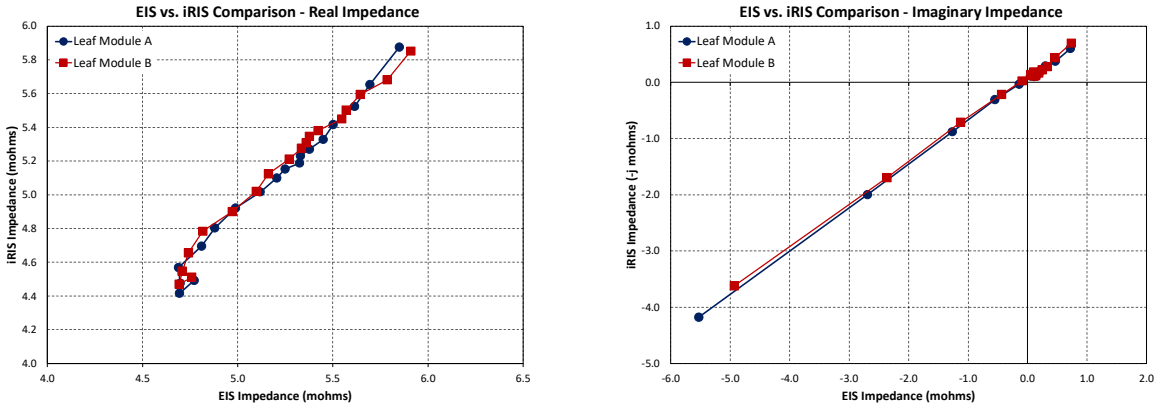


(a) (b)

**Figure 8.** Correlation between EIS and iRIS for (a) real impedance and (b) imaginary impedance

## Summary

The purpose of this paper was to compare iRIS spectra with EIS. Testing demonstrated that iRIS is highly correlated with EIS results over the measured frequency range. EIS took 20 minutes to complete a full sweep, whereas iRIS was 80-s or less. Back-to-back iRIS measurements are also highly reproducible, with faster iRIS measurements (down to 1.25-s) being comparable with the 80-s measurement. Ongoing iRIS development efforts include increased system resolution for enhanced measurements at lower impedance levels and higher voltage capability (up to 100 V).

The iRIS sensor enables broadband impedance measurements at the point of need using non-invasive, repeated field interrogations. The measurement is rapid, benign, and highly correlated with standard EIS measurements. Thus, iRIS opens a new pathway for impedance-based assessments of large production volumes or the generation of in-use datasets for enhanced diagnostics and prognostics. The technology can be incorporated into various stages of the battery life cycle, including cell screening and qualification, cell matching, module/pack end-of-line assessments, field-deployed diagnostics and prognostics, counterfeit detection, and second-use certification.